J|A|C|S ARTICLES

Published on Web 09/24/2010

Controlled Orientation of Polyconjugated Guest Molecules in Tunable Host Cavities

Airon C. Soegiarto, Angiolina Comotti,* and Michael D. Ward*

Department of Materials Science and INSTM, University of Milano Bicocca, Via R. Cozzi 53, 20125 Milan, Italy, and Molecular Design Institute, Department of Chemistry, New York University, 100 Washington Square East, New York, New York 10003-6688, United States

Received July 9, 2010; E-mail: mdw3@nyu.edu

Abstract: Linear conjugated guest molecules with high aspect ratios form inclusion compounds with guanidinium organodisulfonate (GDS) host frameworks in which organodisulfonate "pillars" connect opposing GS sheets to generate lamellar architectures that reflect templating by the guest. Through judicious selection of pillars having adjustable lengths (l_{S-S}, as measured by the separation between distal sulfur atoms) and guests of various lengths (l_g), the framework architecture can be controlled systematically in a manner that enables regulation of the guest orientation and aggregation in the host framework. Inclusion compounds for which $l_g/l_{S-S} \leq 0.9$ exhibit a bilayer architecture with 1-D channels containing guests oriented parallel to the long axis of the pillar. Guests with values of l_g comparable to l_{S-S}, however, promote the formation of a brick architecture in which the guests and the pillar are arranged in a herringbone motif. Surprisingly, longer guests ($l_g = 1.25 l_{S-S}$) favor the formation of the bilayer architecture despite their larger volume because the guests are forced to align end-to-end as single-file arrays due to the vertical constraints of the 1-D channels. Bithiophene and biphenyl guests ($l_g < l_{S-S}$) are exceptional, promoting bilayer structures in which turnstile rotations of the pillars afford an unusual motif in which the guests are isolated from one another. The ability to synthesize a large family of compounds based on a common supramolecular building block (the GS sheet) permits construction of a structural "phase diagram" based on two simple molecular parameters, l_g and l_{S-S}, that can be used to sort the inclusion compounds according to their framework architectures and enable prediction of crystal structures for new host−guest combinations. The effects of these different framework architectures and packing motifs is manifested as bathochromic shifts in the absorption and emission spectra of the guests compared with their spectra in methanol solutions. This behavior is supported by ab initio TDDFT calculations that reproduce the bathochromic shifts associated with the effects of guest−guest and guest−host interactions, combined with conformational constraints imposed on the guest molecules by the rigid host framework.

Introduction

Polyconjugated molecules have substantial potential in electronics, ranging from light-emitting diodes to nonlinear optical devices to thin-film transistors.[1] The optical and electronic properties of these compounds are governed by optical absorption, charge generation, and carrier transport, which typically are cooperative effects that depend on the arrangement of molecular constituents in the solid state.[2] Consequently, the ability to regulate solid-state structure is crucial to advancements in functional molecular crystals. Control of the organization of functional molecules and computational prediction of crystal structure, however, generally has proven elusive owing to the numerous noncovalent interactions that contribute to crystal packing.[3] This limitation has led to a reliance on empirical principles to direct molecular assembly into desired solid-state architectures based on molecular symmetry and structure-directing interactions such as hydrogen bonding or metal coordination.[4,5] One effective strategy involves the use of robust host frameworks that encapsulate functional guest molecules in molecular-scale cavities with tailored shapes, sizes, and

(1) (a) Yang, Y.; Wudl, F. *Adv. Mater.* **2009**, *21*, 1401. (b) Fichou, D. In *Handbook of Oligo-and Polythiophenes*; Wiley-VCH: New York, 1999. (c) Friend, R. H.; Gymer, R. W.; Holmes, A. B.; Burroughes, J. H.; Marks, R. N.; Taliani, C.; Bradley, D. D. C.; Dos Santos, D. A.; Brédas, J.-L.; Lögdlung, M.; Salaneck, W. R. *Nature* **1999**, *397*, 121. (d) Cardin, D. J. *Adv. Mater.* **2002**, *14*, 553. (e) Elemans, J. A. A. W.; van Hameren, R.; Nolte, R. J. M.; Rowan, A. E. *Adv. Mater.* **2006**, *18*, 1251. (f) Katz, H. E.; Bao, Z. *J. Phys. Chem. B* **2000**, *104*, 671. (g) Horowitz, G. *Adv. Mater.* **1998**, *10* (5), 365. (h) Bao, Z.; Rogers, J. A.; Dodabalapur, A.; Lovinger, A. J.; Katz, H. E.; Raju, V. R.; Peng, Z.; Galvin, M. E. *Opt. Mater.* **1999**, *12*, 177. (i) Mitschke, U.; Bäuerle, P. *J. Mater. Chem.* **2000**, *10*, 1471.

(2) Curtis, M. D.; Cao, J.; Kampf, J. W. *J. Am. Chem. Soc.* **2004**, *126*, 4318.

(3) (a) Kitagorodskii, A. I. In *Molecular Crystals and Molecules*; Academic Press: New York, 1973. (b) Bishop, R. *Chem. Soc. Rev.* **1996**, 311–319. (c) Dunitz, J. D.; Gavezzotti, A. *Angew. Chem., Int. Ed.* **2005**, *44*, 1766. (d) Desiraju, G. R. *Acc. Chem. Res.* **2002**, *35*, 565–573.

(4) (a) Jeffrey, G. A. In *An Introduction to Hydrogen Bonding*; Oxford University Press: New York, 1997. (b) Desiraju, G. R.; Steiner, T. In *The Weak Hydrogen Bond in Structural Chemistry and Biology*; Oxford University Press: Oxford, 1999. (c) Russell, V. A.; Etter, M. C.; Ward, M. D. *J. Am. Chem. Soc.* **1994**, *116*, 1941. (d) Moulton, B.; Zaworotko, M. J. *Chem. Rev.* **2001**, *101*, 1629. (e) Hosseini, M. W. *Acc. Chem. Res.* **2005**, *38*, 313. (f) Brammer, L. *Chem. Soc. Rev.* **2004**, *33*, 476. (g) Kitagawa, S.; Kitaura, R.; Noro, S. *Angew. Chem., Int. Ed.* **2004**, *43*, 2234. (h) Yaghi, O. M.; O'Keeffe, M.; Ockiwig, N.; Chae, H. K.; Eddaudi, M.; Kim, J. *Nature* **2003**, *423*, 705.

Scheme 1

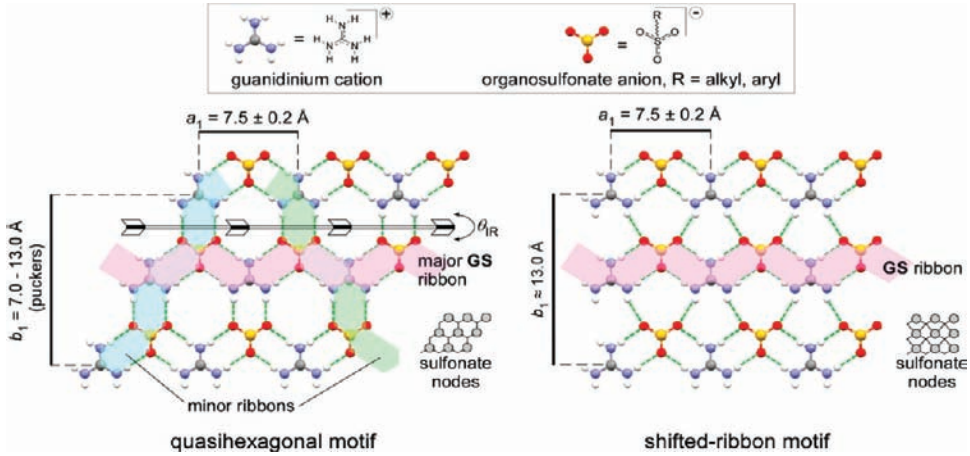

chemical environments that enable systematic regulation of solid state properties.[6−9] This approach promises to simplify the synthesis of molecular materials by decoupling the design of structure, provided by the host framework, from function, introduced by the guest molecules. Furthermore, inclusion of guests in host frameworks can improve their thermal and chemical stability.[10]

While numerous organic host frameworks have been reported,[11] few exist that are amenable to systematic modification with retention of global architecture, thus limiting the inclusion of guest molecules with wide-ranging shapes and sizes in a predictable and reliable manner. Indeed, structural modification of a particular host to accommodate a given guest usually results in unexpected changes in crystal architecture, often with loss of inclusion properties.[12] This obstacle can be surmounted through the use of host frameworks with structurally robust *n*-dimensional supramolecular networks that simplify engineering to the last remaining 3-*n* dimensions and permit the introduction of structural components without loss of architecture.[13] Our laboratory has reported a series of crystalline materials based on guanidinium cations (**G** = $(C(NH_2)_3^+)$ and the sulfonate moieties of organomonosulfonates (**MS**; S = $R\text{-}SO_3^-$)[14] or organodisulfonate anions (**DS**; S = $^-O_3S\text{-}R\text{-}SO_3^-$). The 3-fold symmetry and hydrogen-bonding complementarity of the G ions and S moieties prompt the formation of a two-dimensional (2D) quasihexagonal hydrogen-bonding network (Scheme 1), which has proven to be remarkably robust toward the introduction of various organic pendant groups attached to the sulfonate moieties. The resilience of the GS network simplifies crystal design and synthesis by constraining the crystal packing in two dimensions so that the remaining third dimension can be engineered reliably through the introduction of interchangeable organic groups.[15−18] The organic residues of disulfonates serve as "pillars" that connect opposing GS sheets and enforce the creation of cavities, occupied by guest molecules. The size and chemical character of the cavities can be adjusted through judicious selection of the pillars.[19] The persistence of the 2-D GS network toward the introduction of

(5) (a) Tanaka, K.; Toda, F. *Chem. Rev.* **2000**, *100*, 1025. (b) Macgillivray, L. R.; Papaefstathiou, G. S.; Friscic, T.; Hamilton, T. D.; Bucar, D. K.; Chu, Q.; Varshney, D. B.; Georgiev, I. G. *Acc. Chem. Res.* **2008**, *41*, 280. (c) Farina, M.; Di Silvestro, G.; Sozzani, P. In *Comprehensive Supramolecular Chemistry*; Atwood, J. L.; Davies, J. E. D.; MacNicol, D. D.; Vögtle, F.; Lehn, J.-M., Eds.; Elsevier: Oxford, 1996; Vol. 6; p 371. (d) Yanai, N.; Uemura, T.; Ohba, M.; Kadowaki, Y.; Maesato, M.; Takenaka, M.; Nishitsuji, S.; Hasegawa, H.; Kitagawa, S. *Angew. Chem., Int. Ed.* **2008**, *47*, 9883. (e) Miyata, M. In *Polymerization in Organized Media*; Gordon and Breach Science Publishers: New York, 1992; pp 705−711. (f) van der Boom, T.; Hayes, R. T.; Zhao, Y.; Bushard, P. J.; Weiss, E. A.; Wasielewski, M. R. *J. Am. Chem. Soc.* **2002**, *124*, 9582. (g) Bogani, L.; Sangregorio, C.; Sessoli, R.; Gatteschi, D. *Angew. Chem., Int. Ed.* **2005**, *44*, 5817. (h) Janiak, C. *Dalton Trans.* **2003**, 2781.

(6) (a) Hollingsworth, M. D. *Science* **2002**, *295*, 2410. (b) Irie, M.; Kobatake, S.; Horichi, M. *Science* **2001**, *291*, 1769.

(7) (a) Sozzani, P.; Comotti, A.; Bracco, S.; Simonutti, R. *Angew. Chem., Int. Ed.* **2004**, *43*, 2792. (b) Brustolon, M.; Barbon, A.; Bortolus, M.; Maniero, A. L.; Sozzani, P.; Comotti, A.; Simonutti, R. *J. Am. Chem. Soc.* **2004**, *126*, 15512. (c) Hulliger, J.; Koenig, O.; Hoss, R. *Adv. Mater.* **1995**, *7*, 719. (d) Koenig, O.; Buergi, H.-B.; Armbruster, T.; Hulliger, J.; Weber, T. *J. Am. Chem. Soc.* **1997**, *119*, 10632.

(8) Soegiarto, A. C.; Ward, M. D. *Cryst. Growth Des.* **2009**, *9*, 3803.

(9) (a) Ramamurthy, V.; Caspar, J. V.; Eaton, D. F.; Kuo, E. W.; Corbin, D. R. *J. Am. Chem. Soc.* **1992**, *114*, 3882. (b) Calzaferri, G.; Huber, S.; Maas, H.; Minkowski, C. *Angew. Chem., Int. Ed.* **2003**, *42*, 3732. (c) Berberan-Santos, M. N.; Choppinet, P.; Fedorov, A.; Jullien, L.; Valeur, B. *J. Am. Chem. Soc.* **2000**, *122*, 11876. (d) Li, G.; McGown, L. B. *Science* **1994**, *264*, 249. (e) Wu, C.-G.; Bein, T. *Science* **1994**, *264*, 1757. (f) Spange, S. *Angew. Chem., Int. Ed.* **2003**, *42*, 4430. (g) Aida, T.; Tajima, K. *Angew. Chem., Int. Ed.* **2001**, *40*, 3803. (h) Macchi, G.; Meinardi, F.; Simonutti, R.; Sozzani, P.; Tubino, R. *Chem. Phys. Lett.* **2003**, *379*, 126.

(10) (a) Rahn, M. D.; King, T. A. In *Sol-Gel Optics III*; Mackenzie, J. D., Ed.; (Proceedings of the SPIE) SPIE: Bellingham, WA, 1994; Vol. 2288; pp 382−391. (b) Avnir, D.; Lévy, D.; Reisfeld, R. *J. Phys. Chem.* **1984**, *88*, 5956. (c) Kaminow, I. P.; Stulz, L. W.; Chandross, E. A.; Pryde, C. A. *Appl. Opt.* **1972**, *11*, 1563. (d) Maslyukov, A.; Sokolov, S.; Kaivola, M.; Nyholm, K.; Popov, S. *Appl. Opt.* **1995**, *34*, 1516.

(11) (a) MacNicol, D. D.; Toda, F.; Bishop, R. In *Comprehensive Supramolecular Chemistry*; Pergamon: Oxford, 1996; Vol. 6. (b) Atwood, J. L.; Davies, J. E. D.; MacNicol, D. D. In *Inclusion Compounds*; Academic Press: London, 1991; Vol. 1, 5. (c) Caira, M. R.; Nassimbeni, L. R.; Toda, F.; Vujovic, D. *J. Am. Chem. Soc.* **2000**, *122*, 9367. (d) Hollingsworth, M. D.; Brown, M. E.; Hillier, A. C.; Santarsiero, B. D.; Chaney, J. D. *Science* **1996**, *273*, 1355. (e) Endo, K.; Ezuhara, T.; Koyanagi, M.; Masuda, H.; Aoyama, Y. *J. Am. Chem. Soc.* **1997**, *119*, 499. (f) Brunet, P.; Simard, M.; Wuest, J. D. *J. Am. Chem. Soc.* **1997**, *119*, 2737. (g) Miyata, M.; Tohnai, N.; Hisaki, I. *Acc. Chem. Res.* **2007**, *40*, 694. (h) Bishop, R. *Acc. Chem. Res.* **2009**, *42*, 67. (i) Harris, K. D. M. *Chem. Soc. Rev.* **1997**, *26*, 279. (j) Sozzani, P.; Bracco, S.; Comotti, A.; Ferretti, L.; Simonutti, R. *Angew. Chem., Int. Ed.* **2005**, *44*, 1816. (k) Lim, S.; Kim, H.; Selvapalam, N.; Kim, K. J.; Cho, S. J.; Seo, G.; Kim, K. *Angew. Chem., Int. Ed.* **2008**, *47*, 3352. (l) Comotti, A.; Bracco, S.; Distefano, G.; Sozzani, P. *Chem. Commun.* **2009**, 284.

(12) (a) Schaeffer, W. D. *J. Am. Chem. Soc.* **1957**, *79*, 5870. (b) Williams, F. V. *J. Am. Chem. Soc.* **1957**, *79*, 5876. (c) Caira, M. R.; Horne, A.; Nassimbeni, L. R.; Toda, F. *J. Mater. Chem.* **1997**, *7*, 2145. (d) Caira, M. R.; Horne, A.; Nassimbeni, L. R.; Toda, F. *J. Mater. Chem.* **1998**, *8*, 1481. (e) Caira, M. R.; Nassimbeni, L. R.; Vujovic, D.; Toda, F. *J. Phys. Org. Chem.* **2000**, *13*, 75. (f) Deng, J.; Chi, Y.; Fu, F.; Cui, X.; Yu, K.; Zhu, J.; Jiang, Y. *Tetrahedron: Asymmetry* **2000**, *11*, 1729.

a wide range of organic pillars and guests can be attributed to the existence of charge-assisted N−H···O−S hydrogen bonds as well as several mechanisms for optimizing packing, including an inherent structural compliance of the GS sheet (through puckering), the availability of an alternative "shifted ribbon" motif in which GS ribbons are joined by only a single N−H···O−S hydrogen bond between the cations and anions, and access to multiple architectural isomers characterized by different cavity sizes and shapes.

Cavity metrics and shape depend not only on the molecular structure of the organodisulfonate pillars but also on the arrangement of the pillars between the GS sheets. The GS inclusion compounds exhibit numerous architectures, each endowed with uniquely sized and shaped cavities, with different connectivities between the GS sheets resulting from different "projection topologies" from either side of the 2-D GS sheet.[20] The guest molecules act as steric templates that steer the assembly of the host frameworks toward architectural isomers that optimize host−guest and guest−guest packing.[21] To date, nine unique architectural isomers have been discovered,[8,22,23] the most common being the "bilayer" and the more open "simple brick" (Scheme 2), the latter achieved by templating with larger guest molecules.[21]

GDS inclusion compounds with the bilayer architecture typically confine guests in their 1-D channels such that the long axes of the guests are nominally parallel to the long axis of the organodisulfonate pillar, that is, in a "vertical" orientation, herein denoted as $BL_{||}$ (Scheme 2; the 2-D ordering of the pillars and guests in each architecture, viewed perpendicular to the layers, can be gleaned from the figures contained within Results and Discussion). Guests with larger volumes typically promote the formation of the more open brick frameworks, the most common being the simple brick form. The 1-D channels in the bilayer architecture, however, do not preclude alignment of the long axis of a linear guest perpendicular to the long axis of the supporting pillar provided the guest has a cross section that can be accommodated by the channel. This arrangement, denoted as $BL_{\perp}$, would be more likely for guests with lengths that exceed

Scheme 2

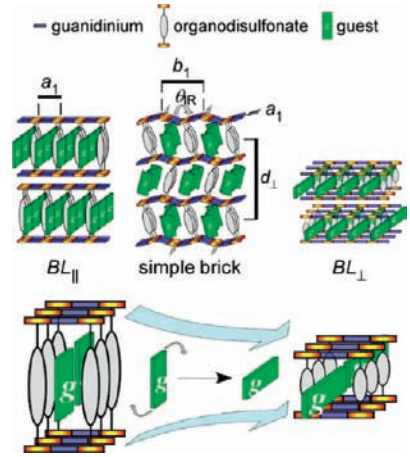

the height of the inclusion cavity, thus frustrating the $BL_{||}$ architecture. Commensurism between the long axis of the guest and the 1-D channel can stabilize the $BL_{\perp}$ architecture further. In principle, because the 1-D channels are effectively infinite, guests of any length, including macromolecules, are potential candidates for inclusion.[24]

We demonstrate herein that the framework architecture of the GDS inclusion compounds and the corresponding arrangement of the linear π-conjugated guest molecules can be regulated through judicious selection of pillar and guest combinations based on their relative lengths rather than their relative volumes. Various guest configurations, edge-to-edge, face-to-edge, end-to-end, were realized by the systematic transition from the $BL_{||}$ to simple brick to $BL_{\perp}$ architecture, achieved with increasing values of the guest length relative to the pillar. This behavior further reveals the role of guest templating and host−guest recognition during host framework assembly but illustrates that guest length can serve as a structure director as well as guest volume. The control of guest arrangement in the solid-state GS frameworks enabled tuning of the optical properties of the guests due to confinement in the host matrix, manifested as bathochromic shifts in the absorption and emission spectra of the guests compared with their spectra in methanol solutions. Ab initio time-dependent density functional theory (TDDFT) calculations reproduce the bathochromic shifts associated with the effects of guest−guest and guest−host interactions, combined with conformational constraints imposed on the guest molecules by the rigid host framework. The ability to direct the orientation of the guest molecules in these frameworks suggests a new route to the design and synthesis of functional materials that require controlled alignment for modulation of electronic properties and solid-state reactivity.

Results and Discussion

Architectural Isomerism and Design. Examination of more than 250 GDS inclusion compounds previously produced in our

(13) (a) Tohnai, N.; Mizobe, Y.; Doi, M.; Sukata, S.; Hinoue, T.; Yuge, T.; Hisaki, I.; Matsukawa, Y.; Miyata, M. *Angew. Chem., Int. Ed.* **2007**, *46*, 2220. (b) Dechambenoit, P.; Ferlay, S.; Kyritsakas, N.; Hosseini, M. W. *J. Am. Chem. Soc.* **2008**, *130*, 17106. (c) Dalrymple, S. A.; Shimizu, G. K. H. *J. Am. Chem. Soc.* **2007**, *129*, 12114. (d) Holman, K. T.; Pivovar, A. M.; Ward, M. D. *Science* **2001**, *294*, 1907. (e) Wang, X.-Y.; Sevov, S. C. *Chem. Mater.* **2007**, *19*, 4906.
(14) Horner, M. A.; Holman, K. T.; Ward, M. D. *J. Am. Chem. Soc.* **2007**, *129*, 14640.
(15) Holman, K. T.; Pivovar, A. M.; Swift, J. A.; Ward, M. D. *Acc. Chem. Res.* **2001**, *34*, 107.
(16) Pivovar, A. M.; Holman, K. T.; Ward, M. D. *Chem. Mater.* **2001**, *13*, 3018.
(17) (a) Russell, V. A.; Etter, M. C.; Ward, M. D. *Chem. Mater.* **1994**, *6*, 1206. (b) Russell, V. A.; Ward, M. D. *J. Mater. Chem.* **1997**, *7*, 1123.
(18) Russell, V. A.; Evans, C. C.; Li, W.; Ward, M. D. *Science* **1997**, *276*, 575.
(19) (a) Swift, J. A.; Reynolds, A. M.; Ward, M. D. *Chem. Mater.* **1998**, *10*, 4159. (b) Evans, C. C.; Sukarto, L.; Ward, M. D. *J. Am. Chem. Soc.* **1999**, *121*, 320.
(20) Holman, K. T.; Martin, S. M.; Parker, D. P.; Ward, M. D. *J. Am. Chem. Soc.* **2001**, *123*, 4421.
(21) Swift, J. A.; Pivovar, A. M.; Reynolds, A. M.; Ward, M. D. *J. Am. Chem. Soc.* **1998**, *120*, 5887.
(22) The various architectural isomers can be distinguished by their "projection topologies", which describe the "up/down" arrangement of the pillars projecting from the sulfonate nodes on the GS sheets. For a detailed discussion, see ref 20.
(23) These architectures include simple bilayer, crisscross bilayer, simple brick, zigzag brick, double brick, V-brick, double zigzag brick, chevron brick, and the chevron bilayer.
(24) (a) Hollingsworth, M. D.; Harris, K. D. M. In *Comprehensive Supramolecular Chemistry*; Elsevier: Oxford, 1996; Vol. 6; p 177. (b) Miyata, M. Inclusion Polymerization. In *Encyclopedia of Supramolecular Chemistry*; Atwood, J. L.; Steed, J. W., Eds.; Marcel Dekker: New York, 2004; Vol. 1; pp 705−711. (c) Sozzani, P.; Comotti, A.; Bracco, S.; Simonutti, R. *Chem. Commun.* **2004**, 768. (d) Comotti, A.; Simonutti, R.; Catel, G.; Sozzani, P. *Chem. Mater.* **1999**, *11*, 1476. (e) Schilling, F. C.; Amundson, K. R.; Sozzani, P. *Macromolecules* **1994**, *27*, 6498. (f) Rusa, C. C.; Wei, M.; Bullions, T. A.; Rusa, M.; Gomez, M. A.; Porbeni, F. E.; Wang, X.; Shin, I. D.; Balik, C. M.; White, J. L.; Tonelli, A. E. *Cryst. Growth Des.* **2004**, *4*, 1431.

Scheme 3

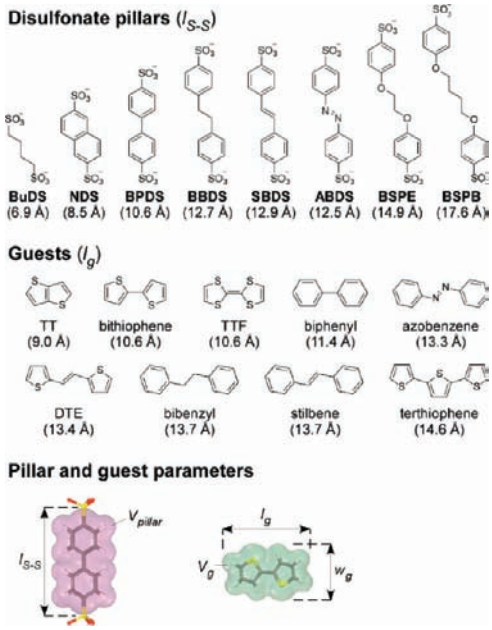

laboratory have revealed an unusual architectural isomerism in which the selectivity for various host framework isomers is governed by the combined steric demands of the organodisulfonate pillars and guest molecules. Each of these isomers is endowed with inclusion cavities having volumes that are determined primarily by the length and the projection topology of the pillars from the GS sheet. Generally, for a given pillar, the framework architecture follows a systematic transition from bilayer to simple brick to "zigzag" brick with increasing guest volume, reflecting increasingly larger inclusion cavity size and the role of guest templating during framework assembly.[15,20] As such, framework isomerism has been viewed primarily in the context of the combined volumes of host pillars and guests, although guest eccentricity (i.e., disk vs oval-shaped) was found to play a role in the selectivity for hexagonal cylindrical host frameworks and lamellar frameworks in GMS inclusion compounds.

The linear π-conjugated molecules used here differ from most guests confined previously in the GDS frameworks by their high aspect ratios (typically >1.6),[25] allowing examination of the influence of guest shape on framework architecture and the corresponding guest aggregation and orientation in the inclusion cavities. This investigation is based on libraries of eight GDS hosts and nine linear π-conjugated guests, characterized by metric variables l_{S-S}, measured by the distance between sulfur atoms in the host pillar, and l_g, the length of the long axis of the guest (Scheme 3). The guest library consisted of 2,2′-bithiophene, biphenyl, *trans*-1,2-di(2-thienyl)ethylene (DTE), *trans*-stilbene, *trans*-azobenzene, bibenzyl, thieno[3,2-*b*]thiophene (TT), 2,2′:5′,2″-terthiophene, and tetrathiafulvalene (TTF), with $9.0 \leq l_g \leq 14.6$ Å. The GDS host library was based on aliphatic and aromatic pillars, with $6.9 \leq l_{S-S} \leq 17.6$ Å. Inclusion compounds derived from these libraries can be classified into three groups according to the l_g:l_{S-S} ratio: (A) l_g:$l_{S-S} \leq 0.92$, (B) $1.00 \leq l_g$:$l_{S-S} \leq 1.10$, and (C) l_g:$l_{S-S} \geq 1.25$ (Table 1). Whereas groups A and B appear to adopt the expected bilayer−simple brick isomerism with guests having larger volumes templating the simple brick form, group C contravenes the expected trend based on guest volume, reverting to the bilayer architecture rather than the zigzag brick form. The bilayer structures in groups A and C adopt the same pillar projection topology, but the orientation of the guests differ with respect to the orientations of the pillars. In group A, the long axis of the guest is nearly parallel to that of the pillar, denoted as $BL_{||}$, whereas in group C the long axis of the guest is nominally perpendicular to that of the pillar, denoted as $BL_{\perp}$ (Scheme 2). Examination of Table 1 reveals a consistent trend of the transition from $BL_{\perp}$ to $BL_{||}$ with increasing l_{S-S} for a common guest, that is, with decreasing l_g:l_{S-S}.

These libraries produced a total of 32 unique inclusion compounds of a possible 72 host−guest combinations (Table 2). The inclusion compounds were crystallized by slow evaporation of methanol solutions containing a unique combination of GDS host and guest, typically resulting in crystals exhibiting a plate-like morphology (see Supporting Information). The observation of 32 inclusion compounds further demonstrates the ability of the GDS hosts to tolerate a wide range of guests, including ones with large aspect ratios. The absence of the inclusion compounds based on the remaining 40 combinations can largely be attributed to pillars that are considerably undersized compared with the dimensional requirements of the larger guests.

$BL_{||}$ Architectures. Twelve GDS inclusion compounds prepared from the libraries in Scheme 3 with l_g:$l_{S-S} \leq 0.92$ were found to template the formation of the $BL_{||}$ architecture, in which the pillars project from the same side, all-up or all-down, of each GS sheet. These compounds consist of those based on the **G_2BPDS** (**BPDS** = 4,4′-biphenyldisulfonate) host with the TT guest, **G_2BSPE** (**BSPE** = 1,2-bis(4-sulfophenoxy)ethane) host with azobenzene, stilbene, bibenzyl, and DTE, **G_2BSPB** (**BSPB** = 1,4-bis(4-sulfophenoxy)butane) host with terthiophene, and **G_2ABDS** (**ABDS** = 4,4′-azobenzenedisulfonate), **G_2SBDS** (**SBDS** = 4,4′-stilbenedisulfonate), and **G_2BBDS** (**BBDS** = 4,4′-bibenzyldisulfonate) hosts with bithiophene, biphenyl, and TTF. The GS sheet in these compounds displays a shifted-ribbon motif rather than quasihexagonal (Scheme 1), producing a lamellar architecture with 1-D channels along b_1 (perpendicular to the GS ribbon; Scheme 1) having a width of 7.3 ± 0.2 Å (3.8 Å when adjusted for van der Waals radii). The formation of the shifted-ribbon motif allows for an expanded channel width compared with that in the quasihexagonal GS motif (6.5 ± 0.2 Å; 3.0 Å when adjusted for van der Waals radii), thus accommodating the guest molecules more readily (see Figure S2, Supporting Information). The heights of the channels are largely determined by the lengths of the pillars, with a secondary contribution from slight tilting.

The guests in the channel are arranged edge-to-edge with their long axes nearly parallel to the pillars, exhibiting face-to-edge contact with the molecular plane of the surrounding pillars (Figure 1A,B). In addition to the size of the pillar, the inclusion cavity volume in the bilayer structure can be influenced by the tilt angle of the pillar with respect to the normal axis of the GS sheet, φ, and the turnstile rotation of the pillar around the C−S bond (Table 1). For a given pillar, a large φ results in shorter bilayer heights and smaller inclusion cavity volumes, which are suitable for guests with smaller volumes. For example, $BL_{||}$ compounds with the **ABDS** pillar reveal an increase of φ from 11.5° for the biphenyl guest (V_g = 155 Å^3) to 13.3° for the bithiophene guest (V_g = 137 Å^3). Similarly, for the **BSPE** pillar

(25) The aspect ratio, l_g/w_g, is determined from the distance between the two most distant atoms along the length (l_g) and width (w_g) of the guest, accounting for the van der Waals radii.

Table 1. Structural Features for GS Inclusion Compounds with the General Formula GDS·*n*(guest)

guest	host	compound no.	framework architecture (θ_{IR})[e]	l_{S-S}(Å)[a]	l_g:l_{S-S}	*n*	nV_g (Å^3)[b]	V_{pillar} (Å^3)[b]	V_{inc} (Å^3)[b]	V_{cell} (Å^3)[c]
TT	**G_2BuDS**	**1**	$BL_\perp$	6.9	1.30	1	108	75	240	516
V_g = 108 Å^3	**G_2NDS**	**2**	simple brick (148.7°)	8.5	1.06	3	324	127	611	921
l_g = 9.0 Å[d]	**G_2BPDS**	**3**	$BL_{||}$	10.6	0.85	1	108	155	254	617
w_g = 6.7 Å[d]										
l_g/w_g = 1.3										
bithiophene	**G_2NDS**	**4**	$BL_\perp$	8.5	1.25	0.5	68	127	212	540
V_g = 137 Å^3	**G_2BPDS**	**5**	simple brick (142.7°)	10.6	1.00	3	411	155	789	1121
l_g = 10.6 Å[d]	**G_2ABDS**	**6**	$BL_{||}$	12.5	0.85	1	137	170	299	682
w_g = 6.5 Å[d]	**G_2BBDS**	**7**	$BL_{||}$	12.7	0.83	1	137	189	320	720
l_g/w_g = 1.6	**G_2SBDS**	**8**	$BL_{||}$	12.9	0.82	1	137	180	310	703
biphenyl	**G_2NDS**	**9**	$BL_\perp$	8.5	1.34	0.5	77	127	231	559
V_g = 155 Å^3	**G_2BPDS**	**10**	simple brick (129.8°)	10.6	1.08	3	465	155	825	1158
l_g = 11.4 Å[d]	**G_2ABDS**	**11**	$BL_{||}$	12.5	0.91	1	155	170	323	705
w_g = 6.4 Å[d]										
l_g/w_g = 1.8										
DTE	**G_2NDS**	**12**	$BL_\perp$	8.5	1.58	0.5	83	127	215	548
V_g = 166 Å^3	**G_2ABDS**	**13**	simple brick (134.9°)	12.5	1.07	3	498	170	927	1279
l_g = 13.4 Å[d]	**G_2BSPE**	**14**	$BL_{||}$	14.9	0.90	1	166	202	368	783
w_g = 6.6 Å[d]										
l_g/w_g = 2.0										
azobenzene	**G_2NDS**	**15**	$BL_\perp$	8.5	1.56	0.5	86	127	226	559
V_g = 173 Å^3	**G_2ABDS**	**16**	simple brick (132.3°)	12.5	1.06	3	519	170	935	1287
l_g = 13.3 Å[d]	**G_2BBDS**	**17**	simple brick (131.0°)	12.7	1.05	3	519	189	958	1325
w_g = 6.5 Å[d]	**G_2SBDS**	**18**	simple brick (135.7°)	12.9	1.03	3	519	180	947	1306
l_g/w_g = 2.0	**G_2BSPE**	**19**	$BL_{||}$	14.9	0.89	1	173	202	376	788
stilbene	**G_2NDS**	**20**	$BL_\perp$	8.5	1.61	0.5	91	127	220	553
V_g = 183 Å^3	**G_2ABDS**	**21**	simple brick (126.7°)	12.5	1.10	3	549	170	963	1315
l_g = 13.7 Å[d]	**G_2BBDS**	**22**	simple brick (127.8°)	12.7	1.08	3	549	189	975	1342
w_g = 6.6 Å[d]	**G_2BSPE**	**23**	$BL_{||}$	14.9	0.92	1	183	202	387	800
l_g/w_g = 2.1										
bibenzyl	**G_2NDS**	**24**	$BL_\perp$	8.5	1.61	0.5	94	127	231	563
V_g = 189 Å^3	**G_2ABDS**	**25**	simple brick (130.7°)	12.5	1.10	3	567	170	964	1317
l_g = 13.7 Å[d]	**G_2BBDS**	**26**	simple brick (134.0°)	12.7	1.08	3	567	189	984	1351
w_g = 6.7 Å[d]	**G_2SBDS**	**27**	simple brick (133.8°)	12.9	1.06	3	567	180	988	1350
l_g/w_g = 2.0	**G_2BSPE**	**28**	$BL_{||}$	14.9	0.92	1	189	202	385	798

[a] l_{S-S} describes the intramolecular separation between distal sulfur atoms in each pillar. [b] Molecular volume (V_g, V_{pillar}, V_{inc}) calculations were performed using Accelrys Materials Studio v.4.2 modeling suite. The volumes of the guest molecules and organodisulfonate pillars, V_g and V_{pillar}, respectively, were obtained using a Connolly (van der Waals) surface using a probe radius of zero and ultrafine grid spacing. The values of V_{pillar} exclude the volume of the sulfonate groups, when combined would contribute 95 Å^3 (average). The volumes tend to be systematically lower, by up to ca. 6%, than those determined by traditional means (see Kitaigorodskii, A. I. In *Molecular Crystals and Molecules*; Academic Press: New York, 1973; pp 18−21). The volumes of each inclusion cavity, V_{inc}, were determined with a Connolly surface using probe radius = 0.5 Å and an ultrafine grid spacing, after removal of guests and normalizing to one host formula unit. [c] V_{cell} values are unit cell volumes obtained from crystallographic data normalized to one host formula unit. [d] The length and width of the guest molecules, l_g and w_g, respectively, correspond to the "major" and "minor" axis of the guests after accounting for van der Waals radii. [e] θ_{IR} values given in this column are applicable for only the simple brick architectures.

φ decreases from 14° for azobenzene (V_g = 173 Å^3) to 8.3° for bibenzyl (V_g = 189 Å^3) to 6.3° for stilbene (V_g = 183 Å^3). Exceptions to this trend were observed, however; for example **G_2BSPE**·(DTE) (φ = 9.7°, V_g = 166 Å^3).

Host frameworks constructed with nonrigid pillars such as **BSPB** can achieve dense packing that reflects conformational flexibility of the pillar. This is evident in the crystal structure of **G_2BSPB**·(terthiophene) in which the central butyl linker of the pillar adopts the gauche-anti-gauche conformation (Figure 2) instead of the all-anti conformation, thus allowing the **G_2BSPB** host framework to shrink-wrap around the terthiophene guest molecule. This compound adopts the quasihexagonal GS sheet motif, producing a 1-D channel, with a width of ca. 6.4 Å (2.9 Å when adjusted for van der Waals radii), along the *b*-axis. These channels would be expected to be too narrow for guest inclusion, but the **BSPB** pillars maximize inclusion cavity volume by distorting and bundling in pairs, to accommodate the guests. Within these channels, the terthiophene guests align with their long axes nearly parallel with the long axis of the pillars, but with a face-to-edge configuration, in contrast with the edge-to-edge configuration of the guest molecules observed in other $BL_{||}$ structures.

Simple Brick Architectures. Thirteen inclusion compounds with l_g:$l_{S-S} \approx 1.0$ adopt simple brick architectures, as illustrated by the **G_2BPDS** host with bithiophene and biphenyl, **G_2NDS** (**NDS** = 2,6-naphthalenedisulfonate) host with TT, and in **G_2ABDS**, **G_2SBDS**, and **G_2BBDS** hosts with azobenzene, stilbene, bibenzyl, DTE, and terthiophene (Figure 3). In contrast to the bilayer structures, which are discrete along the third dimension, the simple brick architectures are continuous in all three dimensions because the pillars project from both sides of each GS sheet, the pillar orientations alternating "up-down" on adjacent GS ribbons. This framework isomerism affords an inclusion cavity volume that is nominally twice that of the corresponding bilayer framework.

The simple brick framework can be described by three mutually orthogonal lattice parameters (Scheme 2),[26] a_1, b_1, $d_\perp$, which essentially idealize the simple brick framework as an orthorhombic lattice. Although deviations from this ideal orthorhombic symmetry are common owing to the softness of the host framework, they typically are slight, resulting in

(26) The lattice parameters b_1 and $d_\perp$ depend on θ_{IR}, according to simple mathematical functions (see ref 15). The $d_\perp$ lattice parameter also depends on the length of the organodisulfonate pillar, l_{S-S}.

Table 2. Crystallographic Data for GS Inclusion Compounds

	G_2BuDS·(TT) **1**	**G_2NDS**·3(TT) **2**	**G_2BPDS**·(TT) **3**	**G_2NDS**·$^1/_2$(bithiophene) **4**
formula	$C_{12}H_{24}N_6O_6S_4$	$C_{30}H_{30}N_6O_6S_8$	$C_{20}H_{24}N_6O_6S_4$	$C_{32}H_{42}N_{12}O_{12}S_6$
formula wt	476.61	827.08	572.69	979.14
crystal system	triclinic	monoclinic	triclinic	triclinic
space group	$P\bar{1}$	$P2_1/n$	$P\bar{1}$	$P\bar{1}$
color	colorless	colorless	colorless	colorless
a (Å)	7.2548(15)	7.6803(5)	7.2917(4)	7.1188(5)
b (Å)	7.5417(16)	20.1103(13)	12.1492(7)	12.3016(9)
c (Å)	11.167(3)	11.9293(8)	15.2108(9)	13.0373(9)
α (deg)	98.349(4)	90	68.0590(10)	81.629(4)
β (deg)	98.643(4)	92.0190(10)	80.6340(10)	75.620(3)
γ (deg)	118.152(3)	90	86.1180(10)	79.022(4)
V (Å^3)	516.0(2)	1841.4(2)	1233.20(12)	1079.89(13)
temp (K)	100(2)	100(2)	100(2)	100(2)
Z	1	2	2	1
R_1 [$I > 2\sigma(I)$]	0.0668	0.0704	0.0475	0.0440
wR_2 [$I > 2\sigma(I)$]	0.1956	0.2170	0.1549	0.1296
G.O.F.	1.149	1.057	1.104	1.045
	G_2BPDS·3(bithiophene) **5**	**G_2ABDS**·(bithiophene) **6**	**G_2BBDS**·(bithiophene) **7**	**G_2SBDS**·(bithiophene) **8**
formula	$C_{38}H_{38}N_6O_6S_8$	$C_{22}H_{26}N_8O_6S_4$	$C_{24}H_{30}N_6O_6S_4$	$C_{24}H_{28}N_6O_6S_4$
formula wt	931.22	626.75	626.78	624.76
crystal system	monoclinic	triclinic	triclinic	triclinic
space group	$P2_1/n$	$P\bar{1}$	$P\bar{1}$	$P\bar{1}$
color	colorless	orange	colorless	brown
a (Å)	7.5783(18)	6.1289(3)	6.1495(5)	6.1517(4)
b (Å)	11.932(3)	7.1528(4)	7.2725(6)	7.2099(5)
c (Å)	24.791(6)	15.7075(8)	16.2688(14)	16.0369(10)
α (deg)	90	93.882(3)	96.933(5)	94.010(4)
β (deg)	90.963(4)	96.130(3)	91.913(5)	96.867(4)
γ (deg)	90	93.115(3)	93.743(5)	93.349(3)
V (Å^3)	2241.4(9)	681.77(6)	720.09(10)	702.85(8)
temp (K)	200(2)	100(2)	100(2)	100(2)
Z	2	1	1	1
R_1 [$I > 2\sigma(I)$]	0.0427	0.0378	0.0347	0.0304
wR_2 [$I > 2\sigma(I)$]	0.1170	0.1071	0.0917	0.0793
G.O.F.	1.119	1.044	1.099	1.04
	G_2NDS·$^1/_2$(biphenyl) **9**	**G_2BPDS**·3(biphenyl)[40] **10**	**G_2ABDS**·(biphenyl) **11**	**G_2NDS**·$^1/_2$(DTE) **12**
formula	$C_{36}H_{46}N_{12}O_{12}S_4$	$C_{50}H_{50}N_6O_6S_2$	$C_{26}H_{30}N_8O_6S_2$	$C_{34}H_{44}N_{12}O_{12}S_6$
formula wt	967.08	−	614.70	1005.17
crystal system	triclinic	monoclinic	triclinic	triclinic
space group	*P*1	$P2_1/n$	$P\bar{1}$	*P*1
color	colorless	colorless	orange	colorless
a (Å)	7.1426(9)	7.6612(6)	6.1627(4)	7.1367(6)
b (Å)	12.7521(15)	26.306(2)	7.2125(5)	12.4838(10)
c (Å)	13.1674(16)	11.4887(9)	16.0535(11)	12.6842(11)
α (deg)	91.845(2)	90	95.2630(10)	83.869(2)
β (deg)	104.765(2)	90.458(2)	94.7580(10)	77.676(2)
γ (deg)	104.145(2)	90	94.6110(10)	85.366(2)
V (Å^3)	1118.8(2)	2315.307	705.31(8)	1095.76(16)
temp (K)	200(2)	173	200(2)	100(2)
Z	1	2	1	1
R_1 [$I > 2\sigma(I)$]	0.0374	0.0359	0.0319	0.0500
wR_2 [$I > 2\sigma(I)$]	0.1095	−	0.0899	0.1557
G.O.F.	1.040	−	1.055	1.187
	G_2ABDS·3(DTE) **13**	**G_2BSPE**·(DTE) **14**	**G_2NDS**·$^1/_2$(azobenzene) **15**	**G_2ABDS**·3(azobenzene) **16**
formula	$C_{44}H_{44}N_8O_6S_8$	$C_{26}H_{32}N_6O_8S_4$	$C_{36}H_{46}N_{14}O_{12}S_4$	$C_{50}H_{50}N_{14}O_6S_2$
formula wt	1037.35	684.82	995.10	1007.16
crystal system	monoclinic	triclinic	triclinic	monoclinic
space group	$P2_1/n$	$P\bar{1}$	*P*1	$P2_1/n$
color	orange	colorless	orange	dark orange
a (Å)	7.573(2)	6.0857(8)	7.1097(5)	7.5750(11)
b (Å)	11.721(4)	7.2198(10)	12.6139(10)	29.220(4)
c (Å)	28.831(9)	18.138(3)	13.8091(11)	11.6324(18)
α (deg)	90	94.606(2)	110.9790(10)	90
β (deg)	91.220(6)	99.461(2)	101.8200(10)	90.103(3)
γ (deg)	90	91.746(2)	93.9510(10)	90
V (Å^3)	2558.7(14)	782.79(18)	1118.01(15)	2574.7(7)
temp (K)	200(2)	200(2)	200(2)	200(2)
Z	2	1	1	2
R_1 [$I > 2\sigma(I)$]	0.0685	0.0376	0.0308	0.0290
wR_2 [$I > 2\sigma(I)$]	0.1961	0.1058	0.1005	0.0825
G.O.F.	1.028	1.069	1.052	1.039

Table 2. Continued

	G_2**BBDS** · 3(azobenzene) **17**	G_2**SBDS** · 3(azobenzene) **18**	G_2**BSPE** · (azobenzene) **19**	G_2**NDS** · $^1/_2$(stilbene) **20**
formula	$C_{52}H_{54}N_{12}O_6S_2$	$C_{52}H_{52}N_{12}O_6S_2$	$C_{28}H_{34}N_8O_8S_2$	$C_{38}H_{48}N_{12}O_{12}S_4$
formula wt	1007.19	1005.18	674.75	993.12
crystal system	monoclinic	monoclinic	triclinic	triclinic
space group	$P2_1/n$	$P2_1/n$	$P\bar{1}$	$P\bar{1}$
color	orange	orange	orange	colorless
a (Å)	7.6405(4)	7.6142(5)	6.1014(4)	7.1176(5)
b (Å)	30.4156(18)	29.502(2)	7.3115(5)	12.5978(8)
c (Å)	11.4061(6)	11.6308(8)	17.9047(13)	12.6173(8)
α (deg)	90	90	91.1680(10)	85.8500(10)
β (deg)	90.7260(10)	90.100(3)	97.0620(10)	87.6160(10)
γ (deg)	90	90	95.9110(10)	78.7700(10)
V (Å^3)	2650.5(3)	2612.7(3)	788.02(9)	1106.34(13)
temp (K)	200(2)	200(2)	200(2)	200(2)
Z	2	2	1	1
R_1 [$I > 2\sigma(I)$]	0.0438	0.0441	0.0346	0.0324
wR_2 [$I > 2\sigma(I)$]	0.1152	0.1051	0.1099	0.1059
G.O.F.	1.026	1.063	1.019	1.043
	G_2**ABDS**·3(stilbene) **21**	G_2**BBDS**·3(stilbene) **22**	G_2**BSPE**·(stilbene) **23**	G_2**NDS**·$^1/_2$(bibenzyl) **24**
formula	$C_{56}H_{56}N_8O_6S_2$	$C_{58}H_{60}N_6O_6S_2$	$C_{30}H_{36}N_6O_8S_2$	$C_{38}H_{50}N_{12}O_{12}S_4$
formula wt	1001.21	1001.24	672.77	995.14
crystal system	monoclinic	monoclinic	triclinic	triclinic
space group	$P2_1/n$	$P2_1/n$	$P\bar{1}$	$P1$
color	orange	colorless	colorless	colorless
a (Å)	7.6038(5)	7.6384(5)	6.0960(4)	7.1652(5)
b (Å)	30.2564(19)	30.908(2)	7.2875(4)	12.5807(10)
c (Å)	11.4283(7)	11.3694(7)	18.3630(11)	25.0454(19)
α (deg)	90	90	97.1930(10)	94.2600(10)
β (deg)	90.0430(10)	90.7390(10)	98.1780(10)	91.0190(10)
γ (deg)	90	90	92.0110(10)	91.2990(10)
V (Å^3)	2629.2(3)	2683.9(3)	799.96(8)	2250.4(3)
temp (K)	200(2)	200(2)	200(2)	200(2)
Z	2	2	1	2
R_1 [$I > 2\sigma(I)$]	0.0368	0.0407	0.0333	0.0459
wR_2 [$I > 2\sigma(I)$]	0.0966	0.0986	0.0907	0.1433
G.O.F.	1.037	1.066	1.038	1.045
	G_2**ABDS**·3(bibenzyl) **25**	G_2**BBDS**·3(bibenzyl) **26**	G_2**SBDS**·3(bibenzyl) **27**	G_2**BSPE**·(bibenzyl) **28**
formula	$C_{56}H_{62}N_8O_6S_2$	$C_{58}H_{66}N_6O_6S_2$	$C_{58}H_{64}N_6O_6S_2$	$C_{30}H_{38}N_6O_8S_2$
formula wt	1007.26	1007.29	1005.27	674.78
crystal system	monoclinic	monoclinic	monoclinic	triclinic
space group	$P2_1/n$	$P2_1/n$	$P2_1/n$	$P\bar{1}$
color	orange	colorless	colorless	colorless
a (Å)	7.7072(6)	7.7503(6)	7.7596(5)	6.1532(8)
b (Å)	29.840(2)	30.182(2)	30.2152(19)	7.2222(10)
c (Å)	11.4574(9)	11.5482(9)	11.5130(7)	18.283(2)
α (deg)	90	90	90	95.493(2)
β (deg)	90.7480(10)	90.583(2)	90.7390(10)	98.852(2)
γ (deg)	90	90	90	92.424(2)
V (Å^3)	2634.8(4)	2701.2(4)	2699.1(3)	797.77(18)
temp (K)	100(2)	173(2)	200(2)	200(2)
Z	2	2	2	1
R_1 [$I > 2\sigma(I)$]	0.0320	0.0435	0.0377	0.0307
wR_2 [$I > 2\sigma(I)$]	0.0847	0.1071	0.0957	0.1006
G.O.F.	1.044	1.028	1.029	1.111
	G_2**ABDS**·(TTF) **29**	G_2**SBDS**·(TTF) **30**	G_2**ABDS**·3(terthiophene) **31**	G_2**BSPB**·(terthiophene) **32**
formula	$C_{20}H_{24}N_8O_6S_6$	$C_{22}H_{26}N_6O_6S_6$	$C_{50}H_{44}N_8O_6S_{11}$	$C_{30}H_{36}N_6O_8S_5$
formula wt	664.83	662.85	1205.59	768.95
crystal system	triclinic	monoclinic	monoclinic	monoclinic
space group	$P\bar{1}$	$C2$	$P2_1/n$	$P2_1/n$
color	dark green	red	orange	light yellow
a (Å)	6.2754(13)	34.320(4)	7.6167(12)	12.3178(7)
b (Å)	7.1880(15)	8.1261(8)	31.632(5)	7.4997(4)
c (Å)	15.396(3)	10.1674(10)	11.2812(17)	38.947(2)
α (deg)	91.838(3)	90	90	90
β (deg)	95.848(3)	99.663(3)	90.604(2)	96.277(2)
γ (deg)	96.074(3)	90	90	90
V (Å^3)	686.4(2)	2795.3(5)	2717.8(7)	3576.4(4)
temp (K)	100(2)	100(2)	200(2)	200(2)
Z	1	4	2	4
R_1 [$I > 2\sigma(I)$]	0.0584	0.0259	0.0432	0.0872
wR_2 [$I > 2\sigma(I)$]	0.1765	0.0709	0.1190	0.2108
G.O.F.	1.186	1.054	1.051	1.076

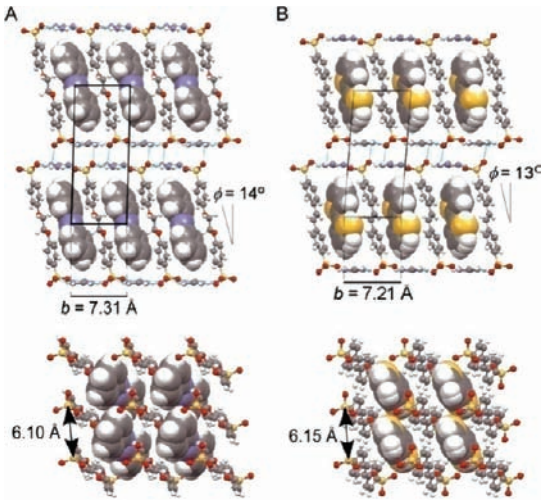

Figure 1. Discrete $BL_{||}$ structures as viewed along the *a* axis (top) and pillar-guest packing as viewed along the *c* axis (bottom) of: (A) G_2**BSPE**·(azobenzene); (B) G_2**SBDS**·(bithiophene). The hosts have been rendered as ball-and-sticks and the guests as space-filling models. In the bottom panel, the **G** ions have been removed for clarity.

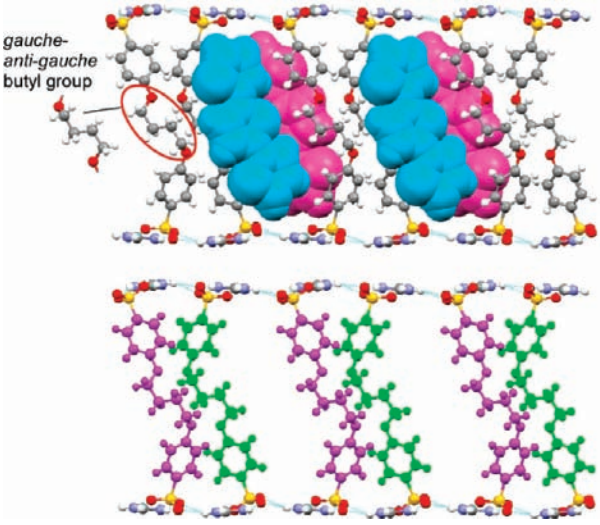

Figure 2. The $BL_{||}$ structure of G_2**BSPB**·(terthiophene) as viewed along the *b* axis. The gauche-anti-gauche conformation adopted by the butyl group of the **BSBP** pillar allows the host framework to densely pack the terthiophene guest molecules, which exhibit face-to-edge configuration in the channel (top). The hosts have been rendered as ball-and-sticks and the guests as space-filling models (colored cyan and pink to aid visualization). In the bottom panel, the guests have been removed to highlight the bundling of the pillars into purple-green pairs.

monoclinic unit cells with β angles near 90°. For example, β = 91.220° and 90.043° for G_2**ABDS**·3(DTE) and G_2**ABDS**·3(stilbene) respectively, due to a modest misregistry of adjacent hydrogen-bonded ribbons along the ribbon direction a_1.

The simple brick inclusion compounds are essentially isostructural with the distribution of the guests and the pillars between the GS sheets organized in a "herringbone" motif (face-to-edge) packing arrangement, a common packing arrangement for aromatic molecules (Figure 4). The 1:3 pillar:guest stoichiometry suggests that the organodisulfonate pillars effectively replace every fourth molecule of the guest in an otherwise guest-only herringbone motif. Whereas the host:guest stoichiometry of the $BL_{||}$ is 1:1, the simple brick architecture typically exhibits 1:3 stoichiometry, larger than that expected for an idealized doubling of the available volume (Table 1). Whereas the bilayer

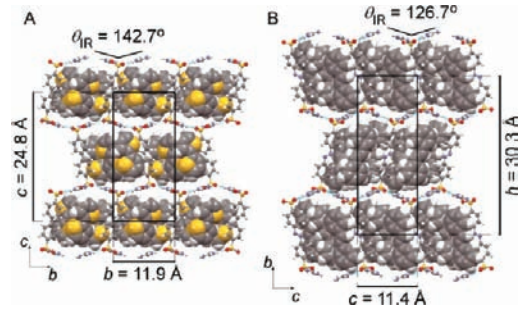

Figure 3. Simple brick structures of (A) G_2**BPDS**·3(bithiophene); (B) G_2**ABDS**·3(stilbene). The hosts have been rendered as ball-and-sticks and the guests as space-filling models.

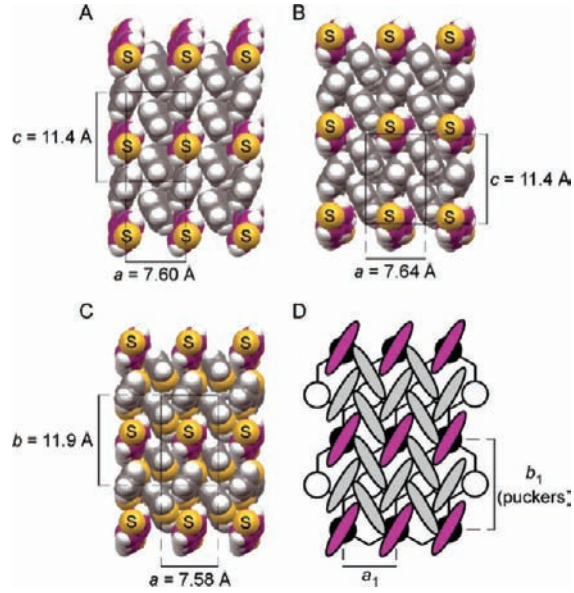

Figure 4. Herringbone (face-to-edge) pillar-guest packing in the *ac* plane of (A) G_2**ABDS**·3(stilbene); (B) G_2**BBDS**·3(azobenzene); (C) G_2**BPDS**·3(bithiophene). The **G** ions and sulfonate oxygen atoms have been removed for clarity. Sulfur atoms are yellow. Carbon atoms of the pillar are purple. Parts A−C are space-filling models. (D) Schematic view, normal to the GS sheet, of the herringbone pillar-guest packing in the simple brick framework, with a 1:3 stoichiometry of pillar (purple) to guest (gray). The pillars projecting below the sheet are depicted as open circles. The herringbone motif resembles the native crystalline packing of the pure guest molecules and that of other aromatic hydrocarbons.

architecture can adjust its inclusion cavity volume slightly through tilting of the pillars, the inclusion cavity volume of the simple brick architecture can adapt to the steric requirements of the guest by puckering about a hydrogen-bond "hinge" joining adjacent GS ribbons, defined by an inter-ribbon puckering angle, θ_{IR} (Scheme 2). When combined with conformational and turnstile-like rotational freedom of the pillars, puckering enables the host framework to shrink-wrap about guest molecules and achieve dense packing. We have demonstrated previously[15] that the maximum inclusion cavity volume is achieved in an ideal simple brick framework when the inter-ribbon puckering angle is approximately 130° rather than 180° (i.e., no puckering). Indeed, in all our simple brick inclusion compounds, the inter-ribbon puckering angles average 130° (Table 1). Interestingly the stilbene and azobenzene moieties in G_2**ABDS**·3(stilbene) and G_2**SBDS**·3(azobenzene) reverse their roles as host and guest. The organic moieties exhibit face-to-edge packing similar to that observed in the herringbone layers of crystalline stilbene or azobenzene. Stilbene and azobenzene molecules in the pure

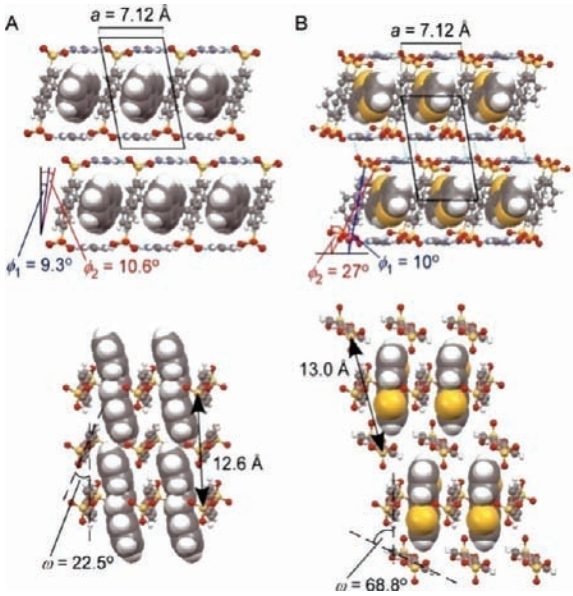

Figure 5. Discrete $BL_{\perp}$ structures as viewed along the *c* axis (top) and pillar-guest packing in the $(\bar{1}\,40)$ plane (bottom) of: (A) $\mathbf{G_2NDS}\cdot{}^1/_2$(stilbene); (B) $\mathbf{G_2NDS}\cdot{}^1/_2$(bithiophene). The hosts have been rendered as ball-and-sticks and the guests as space-filling models. In the bottom panel, the **G** ions have been removed for clarity.

compounds are tilted with respect to the 2-D layers such that the molecules are offset along their long axes by one-half the length of the molecule. The stilbene and azobenzene moieties in the inclusion compounds, however, are not tilted and do not exhibit this offset, revealing structural enforcement on host−guest packing provided by the GS sheet (see Supporting Information).[27]

$BL_{\perp}$ Architectures. Inclusion of π-conjugated molecules with $l_g \geq 1.25\ l_{S-S}$ produced seven compounds that crystallize in a $BL_{\perp}$ architecture (Figure 5), including the $\mathbf{G_2NDS}$ host with azobenzene, bibenzyl, DTE, stilbene, biphenyl, and bithiophene, and the $\mathbf{G_2BuDS}$ (**BuDS** = 1,4-butanedisulfonate) host with TT. The $BL_{\perp}$ architecture differs from previously reported GDS compounds. The long axis of the guests is aligned perpendicular to the long axis of the pillars, such that the long axis of the guests coincides with the channel direction. This reflects a steric frustration of the $BL_{\parallel}$ framework when the pillar is too short to accommodate the guest in the vertical orientation. Consequently, the inclusion compound adopts a configuration in which the guests are arranged end-to-end in a single file along the channel rather than the edge-to-edge configuration observed in the $BL_{\parallel}$ architecture.

The $\mathbf{G_2NDS}$ $BL_{\perp}$ architecture has the same GS sheet projection topology as in the $BL_{\parallel}$ case but with some notable differences. Each guest in the channel spans two periods of the ribbons along the channel direction (the crystallographic *c*-axis in the case of $\mathbf{G_2NDS}\cdot{}^1/_2$(stilbene), Figure 5A; b_1 in Scheme 1), generating an unusual host:guest stoichiometry of 1:0.5. The guest arrays are commensurate with the host lattice (the center-to-center distance of 12.6 Å between aligned guests is double the center-to-center distance between adjacent **NDS** moieties). The 1-D channels of the $BL_{\perp}$ architecture have a rectangular-shaped cross-section of 3.5 × 4.9 Å^2 (calculated on the basis of the crystallographic data and the van der Waals radii), closely matching the cross-section of the guests (as determined by V_g/l_g). Each channel is flanked by nonpolar naphthalene units and polar GS sheets. The $\mathbf{G_2NDS}$ $BL_{\perp}$ architecture creates a cavity environment conducive to host−guest C−H···π contacts ($d_{C-H\cdots\pi}$ = 3.3 − 3.6 Å) while precluding edge-to-edge and face-to-edge guest−guest interactions.

In the $\mathbf{G_2NDS}$ $BL_{\perp}$ architecture, the pillars lining the channel walls display a dihedral angle between the molecular planes of the pillars on alternating adjacent GS ribbons, ω, of approximately 20°. For example, ω = 22.5° for the **NDS** pillars in $\mathbf{G_2NDS}\cdot{}^1/_2$(stilbene) (Figure 5A, bottom). The energy barrier for turnstile rotation around the C−S bond is small (a few kJ/mol, as calculated at the B3LYP/6-311G(d,p) level; see Supporting Information). The resulting conformational freedom allows for facile optimization of host−guest packing, which ranges from guests confined in well-defined channels ($\omega \leq 45°$) to isolated pockets ($\omega > 45°$). Bithiophene and biphenyl guests in the $\mathbf{G_2NDS}$ host adopt the $BL_{\perp}$ architecture, but the 1-D channels are interrupted by the naphthalene moiety of the pillars, which rotate out-of-plane, with ω = 68.8° and 46.5°, respectively (Figure 5B). This configuration effectively encapsulates the guests in cage-like cavities such that they are isolated from one another (Figure 6). This configuration may be a consequence of the smaller length of bithiophene and biphenyl compared with stilbene, azobenzene, and DTE, which are too long to fit inside these cage-like cavities.

The bilayer framework also can maximize packing efficiency through tilting of the pillars with respect to the mean plane of the GS sheet. In the $\mathbf{G_2NDS}$ $BL_{\perp}$ architecture, the tilt of the pillars alternates ribbon-to-ribbon to generate two distinct tilt angles, φ_1 and φ_2, producing GS sheets that are rippled in two dimensions. The φ_1 and φ_2 angles scale inversely with the size of the guest molecules, revealing that the host framework adjusts systematically to the steric requirements of the guests. For example, for the **NDS** pillar, φ_1 and φ_2 decrease from 10° and 27°, respectively, for bithiophene (V_g = 137 Å^3) (Figure 5B, top) to 9.3° and 10.6° for stilbene (V_g = 183 Å^3) (Figure 5A, top).

The TT guest also was included in the shorter $\mathbf{G_2BuDS}$ host with the $BL_{\perp}$ architecture (Figure 7). Due to its small length (l_g = 9 Å, the smallest in the library of Scheme 3), however, TT spans only one ribbon of the GS sheet, forming an inclusion compound with a host:guest ratio of 1:1 instead of 1:0.5. Furthermore, the aliphatic residue of the pillar does not show any dihedral or tilting angle. Although the aspect ratio of TT (1.3) is smaller than the typical values for the other guests in the library, it fits the trend of guest orientation on l_g:l_{S-S} observed for the other inclusion compounds.

The $BL_{\perp}$ architecture is a new occurrence in GDS inclusion compounds. For a given pillar, the GS framework typically prefers the zigzag brick architecture when a guest is too large to fit into the simple brick framework cavities. For example, a pyrene guest with V_g = 187 Å^3 templates the zigzag brick architecture in $\mathbf{G_2NDS}$ host although the volume of pyrene is comparable to that of azobenzene, stilbene, and bibenzyl (Table 1). A similar case is observed for 1-methylnaphthalene; with V_g = 144 Å^3, this guest is nearly the same volume as biphenyl and bithiophene. Both pyrene and 1-methylnaphthalene have

(27) (a) Harada, J.; Ogawa, K. *J. Am. Chem. Soc.* **2004**, *126*, 3539. (b) Chaloner, P. A.; Gunatunga, S. R.; Hitchcock, P. B. *Acta Crystallogr., Sect. C: Cryst. Struct. Commun.* **1994**, *50*, 1941. (c) Bouwstra, J. A.; Schouten, A.; Kroon, J.; Helmholdt, R. B. *Acta Crystallogr., Sect. C: Cryst. Struct. Commun.* **1985**, *41*, 420. (d) Ruban, G.; Zobel, D. *Acta Crystallogr., Sect. B: Struct. Crystallogr. Cryst. Chem.* **1975**, *31*, 2632. (e) Harada, J.; Ogawa, K. *Struct. Chem.* **2001**, *12*, 243. (f) Charbonneau, G.-P.; Delugeard, Y. *Acta Crystallogr., Sect. B: Struct. Crystallogr. Cryst. Chem.* **1977**, *33*, 1586.

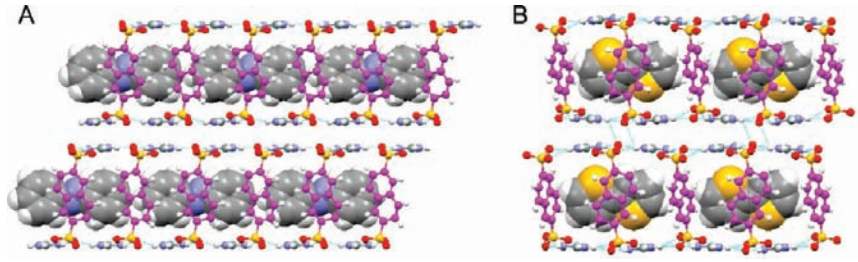

Figure 6. (A) The end-to-end arrangement of the azobenzene guests in the 1-D channels of the $BL_{\perp}$ $\mathbf{G_2NDS}\cdot{}^1/_2$(azobenzene) as viewed along the *a* axis. (B) Completely isolated bithiophene guests nestled within the "cage"-like cavity of the $BL_{\perp}$ $\mathbf{G_2NDS}\cdot{}^1/_2$(bithiophene) as viewed along the *a* axis. In both cases, the long axis of the guests is nearly orthogonal to that of the pillar. The hosts have been rendered as ball-and-sticks and the guests as space-filling models. In addition, the carbon atoms of the **NDS** pillars are colored purple to aid visualization.

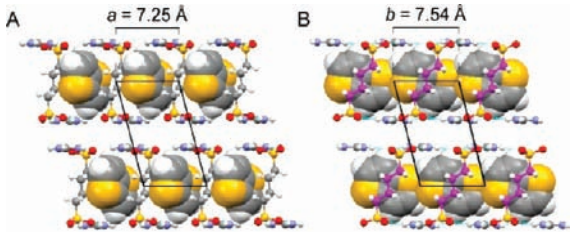

Figure 7. $BL_{\perp}$ structure of $\mathbf{G_2BuDS}\cdot$(TT) as viewed along: (A) the *b* axis or the channel direction; (B) the *a* axis highlighting the end-to-end configuration of the TT guests. The hosts have been rendered as ball-and-sticks and the guests as space-filling models. In addition, the carbon atoms of the **BuDS** pillars in (B) are colored purple to aid visualization.

an aspect ratio of 1.2, which is much smaller than those of the elongated guests herein studied (from 1.6 to 2.1, with the exception of TT). This implies that the formation of the $BL_{\perp}$ structure can be attributed to the high aspect ratio of the guests, which steers templating of 1-D channels while frustrating the zigzag brick framework, which does not have 1-D cavities due to the zigzag arrangement of adjacent GS ribbons. This phenomenon further reinforces the role of guest-templating effects in GS framework assembly, not unlike the templating mechanism proposed for the formation of zeolite and inorganic networks.[28]

Structural Phase Diagram. The GDS hosts can form a variety of lamellar architectures, each endowed with inclusion cavities of different sizes and shapes, exhibiting conformational flexibility that permit the optimization of the host−host and host−guest interactions and thus the accommodation of a wide variety of guests in the voids. The discovery of a new arrangement of the guest with respect to the hosts, realized by varying the length of the organic groups, reveals the inherent ability of these compounds to optimize packing while retaining the hydrogen-bond connectivity of the GS sheet and the overall lamellar organization. Using l_g and l_{S-S}, a "structural phase diagram"[14] (Figure 8) can be constructed to illustrate the relationship between simple, well-defined molecular parameters and the host framework architecture of the inclusion compounds. Figure 8 describes the positions of 59 inclusion compounds on this diagram, including new compounds reported herein (filled symbols) as well as others reported previously that contain polyacene guests (unfilled symbols), which also are rigid and conjugated. The phase diagram reveals that the different architectures are located in distinct sectors according to their l_g/l_{S-S} ratios.

Previously reported GDS inclusion compounds in Figure 8 (unfilled symbols), which were restricted to guests with l_g:l_{S-S} < 1.25, typically reside in the two rightmost sectors, illustrating the general trend from the $BL_{||}$ to the simple brick architecture with increasing guest volume, relative to the pillar volume, as well as increasing l_g:l_{S-S}. These compounds, which consist of polyacene pillars **NDS**, **BPDS**, and **ADS** (2,6-anthracenedisulfonate) (l_{S-S} = 8.5, 10.6, and 10.8 Å, respectively), crystallize as either the $BL_{||}$ or simple brick, depending on the relative sizes of the pillars and guests. Generally, pillars without bulky substituents favor bilayer frameworks when small guests are included, whereas brick frameworks are templated by large guests. The transition from $BL_{||}$ to simple brick resulting from increases in l_g:l_{S-S} is apparent by inspection of Figure 8. For example, the $\mathbf{G_2BPDS}$ host forms the $BL_{||}$ architecture with guests having 9.1 ≤ l_g ≤ 10.4 Å, including monosubstituted naphthalene guests $C_{10}H_7X$ (X = Br, Cl, CH_3) and 1,2- and 1,5-dimethylnaphthalene. The simple brick architecture, however, is observed for guests having 10.7 ≤ l_g ≤ 11.6 Å as well as monosubstituted naphthalenes bearing bulkier substituents such as $C_{10}H_7X$ (X = I, NO_2, CN) and the remaining eight dimethylnaphthalenes.[21] Similarly, the $\mathbf{G_2ADS}$ host forms the $BL_{||}$ architecture for guests such as naphthalene and tetrathiafulvalene (l_g = 9.2 and 10.6 Å, respectively) but the simple brick architecture for larger guests such as pyrene, anthracene,

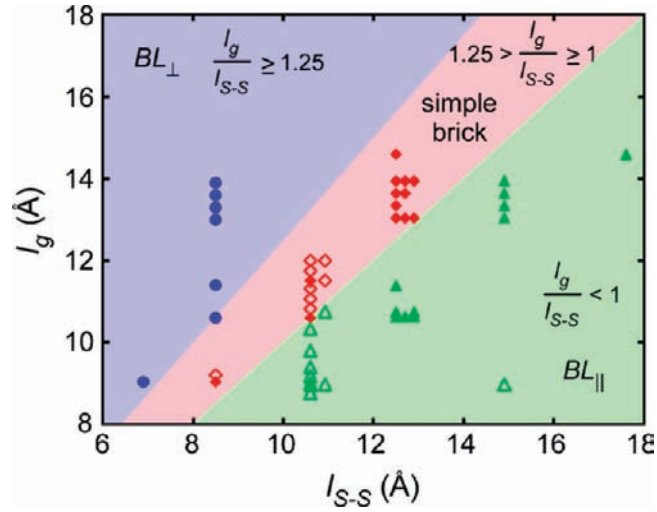

Figure 8. Structural phase diagram for GDS inclusion compounds sorted according to distinct sectors defined by the value of l_g:l_{S-S}. Blue circles (●) denote $BL_{\perp}$ compounds, red diamonds (♦, ◊) denote simple brick compounds, and green triangles (▲, Δ) denote $BL_{||}$ compounds. Filled symbols (♦, ▲, ●) refer to 32 inclusion compounds reported herein and unfilled symbols (◊, Δ) refer to 27 inclusion compounds that had been previously reported and were formed with polyacene-based guests. The diagram actually contains 59 entries, but only 49 are visible because several compounds overlap.

(28) Davis, M. E.; Katz, A. J.; Ahmad, W. R. *Chem. Mater.* **1996**, *8*, 1820.

Table 3. Absorption (λ_{max}) and Emission (λ_{em}) Wavelengths and Stokes Shift ($\lambda_{em} - \lambda_{max}$) for the Inclusion Compounds

compound	architecture	λ_{max} (nm)	λ_{em} (nm)	$\lambda_{em} - \lambda_{max}$ (nm)
G_2NDS·$^1/_2$(bithiophene)	$BL_\perp$	335	431	96
G_2BPDS·3(bithiophene)	simple brick	336	384	48
G_2BBDS·(bithiophene)	$BL_{||}$	334	372	38
bithiophene	−	307	391	84
bithiophene (in MeOH)	−	302	358	56
G_2NDS·$^1/_2$(stilbene)	$BL_\perp$	338	396	58
G_2BBDS·3(stilbene)	simple brick	336[a]	384	48
G_2BSPE·(stilbene)	$BL_{||}$	332[a]	375	43
stilbene	−	317	410	93
stilbene (in MeOH)	−	307[a]	346	39
G_2NDS·$^1/_2$(azobenzene)	$BL_\perp$	330[b]	387	57
G_2BBDS·3(azobenzene)	simple brick	332[b]	353	21
G_2BSPE·(azobenzene)	$BL_{||}$	332[b]	355	23
azobenzene	−	318[b]	349	31
azobenzene (in MeOH)	−	317[b]	348	31

[a] This λ_{max} value corresponds to the electronic transition with the longest wavelength. Other absorption maxima with roughly equal intensities to that of λ_{max} are present at 318, 302, and 290 nm in the spectra. [b] Another absorption maxima with much lower intensities than that of λ_{max} are present at about 445 nm.

and biphenyl ($l_g \approx 11.5$ Å). The simple brick architecture is also preferred in isostructural host−guest combinations, **G_2NDS**·3(naphthalene), **G_2BPDS**·3(biphenyl), and **G_2ADS**·3(anthracene), with herringbone pillar-guest packing that mimic the layer motifs in the crystals of their respective pure guests.[20] These structures reveal that dependence of the selectivity for $BL_{||}$, and simple brick architectures can be explained by l_g:l_{S-S} as well as V_g:V_{pillar}. In contrast, the examples in the $BL_\perp$ sector can only be explained by l_g:l_{S-S}.

Figure 8 includes examples for which only two of the three architectures were observed for a common guest, specifically inclusion compounds containing terthiophene or TTF guests (Table S1, Supporting Information). Terthiophene forms the $BL_{||}$ architecture with **ABDS** and **SBDS** hosts. In the case of **G_2ABDS**·(TTF), the $\pi-\pi$ stacking between **ABDS** and TTF imparts a dark green color due to formation of a charge-transfer complex[29] wherein **ABDS** is the electron acceptor and TTF the electron donor.

A more expansive structural phase diagram constructed from a more diverse set of pillar−guest combinations (>250 GDS inclusion compounds) exhibits similar architectural sorting, although the phase boundaries are not as distinct as in Figure 8 (Figure S5, Supporting Information). Nonetheless, these structural phase diagrams illustrate that architectural isomers sharing a common supramolecular building block, in this case the two-dimensional GS sheets, can be sorted according to simple molecular parameters, promising structure prediction for untested host−guest combinations.

Optical Properties of the Photoactive Guests Included within the GDS Hosts. The three framework isomers described above result in distinct guest−guest aggregation and host−guest packing motifs, which can be expected to influence the optical absorption and emission of the guests confined within the framework cavities. This can only be demonstrated for inclusion compounds based on a host and guest without overlapping absorption and emission bands as in the combinations of **G_2NDS**, **G_2BPDS**, **G_2BBDS**, and **G_2BSPE** hosts and bithiophene, stilbene, and azobenzene guests (Table 3). The absorption bands of these guests in the GDS host frameworks, regardless of architecture, exhibit bathochromic shifts (i.e., red-shifted) compared with the absorption maxima in solution (<10^{-5} M). The bathochromic shifts are the result of the balance among various factors, including the increase of effective conjugation length associated with molecular geometry (i.e., planar vs nonplanar) as well as host−guest and guest−guest interactions. The influence of these factors on the electronic transitions of the guests was investigated by performing ab initio calculations. The electronic transition energies of the conjugated guests, as encapsulated in the various inclusion frameworks, and as isolated molecules or molecular aggregates (with structures extracted from the crystal structures of the inclusion compounds), were calculated using time-dependent density functional theory (TDDFT), which is regarded as a reliable computational method for evaluating the ground and low-lying excited state spectrum of conjugated molecules,[30] at the PBE0/6-311G(d,p) level. The PBE0 hybrid functional is extremely efficient for accurately reproducing experimental values and absorption spectra in several applications.[31]

The bithiophene guests in **G_2NDS**·$^1/_2$(bithiophene) exhibited an experimentally measured bathochromic shift of 33 nm in the absorption wavelength (λ_{max}) compared with λ_{max} for bithiophene alone in methanol. The influence of host−guest interactions on the optical properties were calculated using an inclusion compound environment mimicking the packing arrangements of the guest molecules within the cavities, as determined by single crystal X-ray diffraction of the inclusion compound. Bithiophene guests in the **G_2NDS** host framework reside in cage-like cavities, largely isolated from one another, surrounded by **NDS** pillars and GS sheets (Figure 6B). The calculations for bithiophene confined in the cage-like cavity of **G_2NDS**·$^1/_2$(bithiophene), which is formed by four **NDS** and four **G** moieties, revealed an electronic transition at $\lambda_{max,calc} = 330$ nm (see Supporting Information), in excellent agreement with the experimental data ($\lambda_{max} = 335$ nm).[32] The calculated electronic transition wavelength is red-shifted by 28 nm compared to that calculated for the isolated guest molecule, comparing favorably with the aforementioned shift observed experimentally and supporting the importance of host−guest interactions.

The experimentally observed bathochromic shift (7 and 13 nm, based on $\lambda_{max} = 324$ and 330 nm) for azobenzene in the **G_2NDS** host matched the shift of 5 and 12 nm (based on $\lambda_{max,calc} = 321$ and 328 nm) calculated for a single azobenzene guest surrounded by four **NDS** and four **G** moieties of the **G_2NDS** host. Similarly, the experimental bathochromic shift for *trans*-

(29) Evans, C. C. Confinement of Dyes in Nanometer-Scale Domains. Ph.D. Dissertation, University of Minnesota, Minneapolis, MN, 1998.

(30) Runge, E.; Gross, E. K. U. *Phys. Rev. Lett.* **1984**, *52*, 997.

(31) (a) Perdew, J. P.; Burke, K.; Ernzerhof, M. *Phys. Rev. Lett.* **1996**, *77*, 3865. (b) Adamo, C.; Barone, V. *J. Chem. Phys.* **1999**, *110*, 6158. (c) Cossi, M.; Barone, V. *J. Chem. Phys.* **2001**, *115*, 4708. (d) Jacquemin, D.; Preat, J.; Wathelet, V.; Fontaine, M.; Perpète, E. A. *J. Am. Chem. Soc.* **2006**, *128*, 2072. (e) Santoro, F.; Lami, A.; Improta, R.; Barone, V. *J. Chem. Phys.* **2008**, *128*, 224311.

(32) The bithiophene guests in the inclusion compounds are trans-planar with the dihedral (S−C−C−S) angle of 180°. Computations reveal that the torsional energy barrier between two bithiophene conformers with a dihedral (S−C−C−S) angle of 150° (the minimum) and 180° (trans-planar) is approximately 0.3 kcal/mol ($\sim 0.5Nk_BT$ at room temperature). The maximum energy barrier, between two conformers with a dihedral (S−C−C−S) angle of 150° and 90°, was calculated to be approximately 2 kcal/mol ($\sim 3Nk_BT$ at room temperature). These relatively small barriers suggest that multiple conformers coexist in solution and in the gas phase (Figure S8, Supporting Information). Also see: (a) Takayanagi, M.; Gejo, T.; Hanazaki, I. *J. Phys. Chem.* **1994**, *98*, 12893. (b) Chadwick, J. E.; Kohler, B. E. *J. Phys. Chem.* **1994**, *98*, 3631.

stilbene in **G**$_2$**NDS** (31 nm; $\lambda_{max} = 338$ nm) is in good agreement with the shift of 17 and 29 nm calculated for a single stilbene guest in the same host environment.[33,34] Formation of *J*-type aggregates, in which neighboring molecules adopt a head-to-tail arrangement, also should be considered because they are often associated with bathochromic shifts compared with the isolated molecules.[35] These shifts have been explained by molecular exciton theory, which invokes coupling of transition moments between neighboring molecules that splits the lowest singlet excited state (Davydov splitting). The transition to the lower Davydov level, which is responsible for the bathochromic shift, is optically allowed for *J*-type aggregates whereas the transition to the upper Davydov level is optically forbidden. In the case of stilbene and azobenzene in **G**$_2$**NDS** host (with BL$_\perp$ architecture), the guests align end-to-end along the 1-D channel, like *J*-type aggregates (Figure 6A). Notably, calculations revealed small bathochromic shifts of ~3 and 5 nm, respectively, for pairs of azobenzene and stilbene guests (without the host) having the *J*-aggregate-like motifs observed in their respective inclusion compounds. The relatively small shifts calculated for the *J*-aggregate-like motifs further supports an important role for host−guest interactions in the optical properties and only a minor contribution to the optical properties from guest−guest interaction. Interestingly, the influence of the host is dramatic compared with typical solvents, as the effect of solvent polarity on λ_{max} is negligible (as measured in hexane, cyclohexane, benzene, acetonitrile, and methanol).[36] Attempts to compare the optical properties for bithiophene, azobenzene, and stilbene guests included within the BL$_{||}$ architecture and their host-free molecular or aggregate forms were precluded by the large number of atoms to be considered in the computationally demanding high-level TDDFT methods.[37]

The emission wavelength (λ_{em}) for guests in the GDS host frameworks also exhibit bathochromic shifts compared with their respective values in dilute solutions (Figure 9). The largest shifts were recorded for bithiophene, stilbene, and azobenzene guests confined within hosts having the BL$_\perp$ architecture. For example, a bathochromic shift of 73 nm ($\lambda_{em} = 431$ nm) was observed for bithiophene in **G**$_2$**NDS** host (BL$_\perp$), compared with λ_{em} in any of the aforementioned solvents. In contrast, bithiophene in **G**$_2$**BPDS** (simple brick) and **G**$_2$**BBDS** (BL$_{||}$) hosts exhibited a bathochromic shift of only 36 and 14 nm, respectively. The emission bands of bithiophene and azobenzene guests in their respective inclusion compounds are broad and featureless. Stilbene guests exhibit multiple peaks corresponding to electronic relaxation to different vibrational energy levels of the ground state in **G**$_2$**BBDS** and **G**$_2$**BSPE**, but broad featureless bands in **G**$_2$**NDS**.[38] Curiously, the Stokes shift, the difference between the absorption and emission maxima, is larger for the chromophores embedded in the inclusion compounds compared with their respective values in solution. This may seem surprising, as the magnitude of the Stokes shift usually increases for molecules due to geometry changes or solvent reorganization,[39] which would be expected to be less in the constrained environment of the solid-state host than in solution. The chromophores examined here, however, lack substantial dipolar character, which would be expected to produce small Stokes

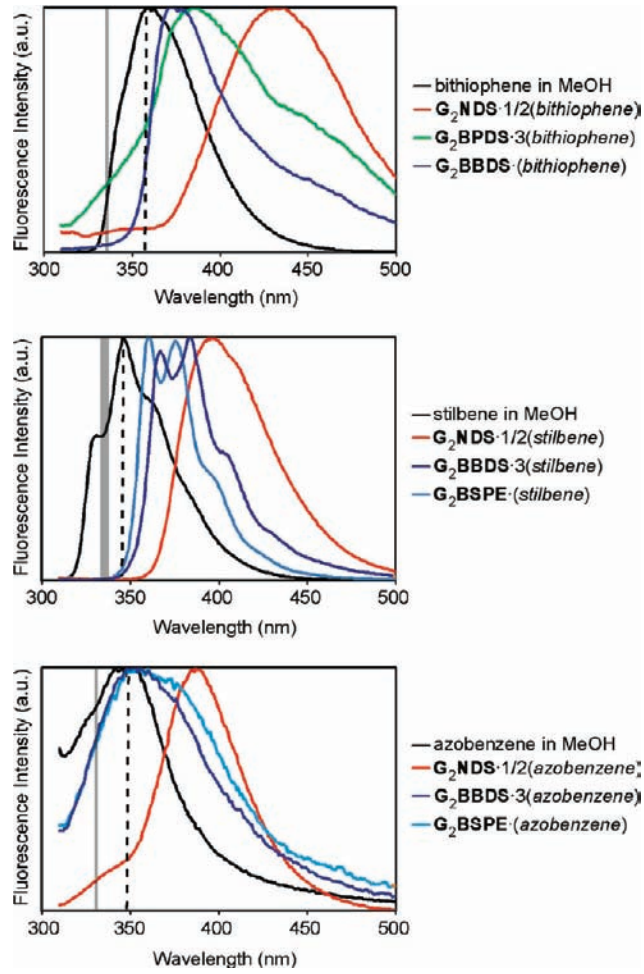

Figure 9. The photoluminescence spectra of bithiophene, *trans*-stilbene, and *trans*-azobenzene in various GDS host frameworks. The spectra of the guests alone dissolved in methanol (10^{-5} M) are provided for comparison. The bathochromic shift can be gleaned from the λ_{em} values (emission) in methanol, denoted by the vertical dashed line. All intensity values are normalized. The range of λ_{max} values (absorption) for each guest chromophore in the inclusion compounds is denoted by the vertical gray band. The actual λ_{max} values are provided in Table 3.

(33) (a) Chen, P. C.; Chieh, Y. C. *J. Mol. Struct. (THEOCHEM)* **2003**, *624*, 191. (b) Brown, E. V.; Granneman, G. R. *J. Am. Chem. Soc.* **1975**, *97*, 621. (c) Champagne, B. B.; Pfanstiel, J. F.; Plusquellic, D. F.; Pratt, D. W.; van Herpen, W. M.; Meerts, W. L. *J. Phys. Chem.* **1990**, *94*, 6.

(34) The minimum energy conformation for free *trans*-stilbene and *trans*-azobenzene is reported as planar, as found in the GDS inclusion compounds. Consequently, the contribution of conformational effects to the bathochromic shifts for these compounds is negligible.

(35) Cornil, J.; Beljonne, D.; Calbert, J.-P.; Brédas, J.-L. *Adv. Mater.* **2001**, *13*, 1053.

(36) A small red shift (<2 nm) has been reported for bithiophene with increasing solvent polarity. See: (a) Di Césare, N.; Belletête, M.; Raymond, F.; Leclerc, M.; Durocher, G. *J. Phys. Chem. A* **1997**, *101*, 776. (b) Meng, S.; Ma, J.; Jiang, Y. *J. Phys. Chem. B* **2007**, *111*, 4128.

(37) Although computations for a complete inclusion cavity based on four **BBDS** pillars, four **G** ions, and a single bithiophene guest were not possible due to the large number of atoms involved, calculation with a lower number of host molecules (four **BBDS** pillars, two **G** ions) and one guest revealed a bathochromic shift of 14 nm, much less than the experimental value of 32 nm. Calculation at the same level predicted a hypsochromic shift (blue-shift) of ~3 nm for two bithiophene guests (without host) with the edge-to-edge motif observed in the **G**$_2$**BBDS** inclusion compound. These results further reinforce a more important role for host−guest interactions in the bathochromic shifts compared with guest−guest interactions.

(38) Waldeck, D. H. *Chem. Rev.* **1991**, *91*, 415.

(39) Anslyn, E. V.; Dougherty, D. A. In *Modern Physical Organic Chemistry*; University Science Books: Sausalito, 2006; pp 942−946.

(40) CSD Reference Code MAXZUG Holman, K. T.; Ward, M. D. *Angew. Chem., Int. Ed.* **2000**, *39*, 1653.

shifts regardless of the environment. This is supported by the observation of a negligible dependence of λ_{em} for each guest on the polarity of the solvent (hexane, cyclohexane, benzene, acetonitrile, methanol). This suggests that other factors contribute to the energetic relaxation of the excited state and the associated Stokes shifts in the inclusion compounds, possibly coupling of the excited state with lattice phonons or with the excited states of other guest chromophores, which could be enhanced by the degree of guest alignment and small intermolecular distances in the solid state compared with dilute solutions.

Conclusions

The architecture of GDS host frameworks and the orientation of linear π-conjugated guest molecules in 1-D channels can be regulated systematically based on the relative lengths of the pillar and the guest. Increasing values of l_g:l_{S-S} are accompanied by a systematic transition in the framework architecture from the $BL_{||}$ to simple brick to $BL_{\perp}$, and consequently, a change in the aggregation motifs of the confined guests from edge-to-edge to face-to-edge to end-to-end. The framework architecture types can be sorted in a "structural phase diagram" according to simple molecular parameters, l_g and l_{S-S}, which can be used for structure prediction in this class of compounds. Although the $BL_{||}$ and simple brick architectures have been well documented in the past, the formation of the $BL_{\perp}$ architecture (with $l_g \geq 1.25\ l_{S-S}$) is unprecedented and appears to be associated with guests having high aspect ratios. The $BL_{\perp}$ architecture can generate either a 1-D channel or a cage-like cavity depending on the length of the confined guests; for example, stilbene guests in **G$_2$NDS** host ($BL_{\perp}$; l_g:$l_{S-S} = 1.61$) are arranged end-to-end along the 1-D channel whereas bithiophene guests in the same host ($BL_{\perp}$; l_g:$l_{S-S} = 1.25$) are isolated in cage-like cavities. The effects of the various host and/or guest aggregation motifs on the optical properties of the confined guests are manifested in the bathochromic shifts in the absorption and emission spectra relative to those in dilute solution. The shifts in the absorption bands were corroborated by ab initio computations (using TDDFT at the PBE0/6-311G(d,p) level) based on the structures of the host−guest aggregates observed in the crystalline state. The ability of the GDS hosts to adapt to different size and shape requirements of the guests by forming various architectures that can be sorted according to simple molecular parameters reveals the exceptional capability of these hosts for regulating guest aggregation in a reliable and predictable manner. Additionally, the host components in GDS compounds are often π-conjugated and, therefore, may contribute to energy and charge transfer processes in a manner that modulates the optical properties derived from the confined guests. Collectively, these features suggest promising pathways to the design and synthesis of functional materials.

Experimental Section

Materials and General Procedures. Guanidine carbonate salt, tetrafluoroboric acid, 2,6-naphthalenedisulfonic acid disodium salt, Amberlyst 36 (wet) ion-exchange resin, 2,2′-bithiophene, bibenzyl, azobenzene, *trans*-stilbene, biphenyl, 2,2′:5′,2″-terthiophene, and tetrathiafulvalene were purchased from Sigma-Aldrich (Milwaukee, WI). 4,4′-Biphenyldisulfonic acid and thieno[3,2-b]thiophene were purchased from TCI America (Tokyo, Japan). These chemicals were used without further purification. **G$_2$BBDS** and **G$_2$BSPE** apohosts,[8] the sodium salt of 4,4′-azobenzenedisulfonate,[41] the sodium salt of 4,4′-disulfostilbene,[42] and the sodium salt of 1,4-butanedisulfonate[43] were prepared according to published procedures. All solvents and other starting materials were purchased as ReagentPlus or ACS reagent grade from Aldrich, Acros (Geel, Belgium), or Alfa Aesar (Ward Hill, MA) and were used as received. Metal salts of the sulfonic acids were converted to the acid form by passing them through an Amberlyst 36(wet) ion-exchange column. **G$_2$NDS**, **G$_2$BPDS**, **G$_2$ABDS**, **G$_2$SBDS**, and **G$_2$BuDS** precipitate, as acetone clathrates, by direct reaction of guanidinium tetrafluoroborate, prepared by neutralization of guanidinium carbonate with tetrafluoroboric acid, with the corresponding disulfonic acid in acetone. These compounds readily lose enclathrated acetone under ambient conditions to yield pure guanidinium organodisulfonate apohosts. The inclusion compounds reported here were crystallized from methanolic solutions (by slow evaporation method) containing the dissolved apohost and the corresponding guest where applicable. The stoichiometries of the resulting inclusion compounds tend to be independent of the host:guest stoichiometric ratios during crystallization. The stoichiometries of all inclusion compounds were confirmed by ^{1}H NMR spectroscopy in addition to single-crystal structure determinations. ^{1}H NMR spectra were recorded on a Bruker AV-400 spectrometer operating at 400 MHz.

[Guanidinium]$_2$[1,4-bis(4-sulfophenoxy)butane], G$_2$BSPB. An ethanolic solution containing 1:1 molar ratio of NaOH (1.72 g, 43 mmol) and 4-hydroxybenzenesulfonic acid sodium salt dihydrate (10 g, 43 mmol) was prepared and refluxed for 30 min. 1,4-Dibromobutane (4.64 g, 21.5 mmol) was then added to the solution, and the reaction was left to reflux for a further 100 h. After the reaction ended, the mixture was rotary-evaporated to remove the ethanol solvent. The remaining solid residue, which contained the sodium salt of **BSPB**, was dissolved in water and converted to the acid form by passing them through an Amberlyst 36(wet) ion-exchange column. After the water had been rotary-evaporated, the **BSPB** acid was dissolved in acetone and then treated with an acetone solution of **G**[BF_4]. The **G$_2$BSPB**·(acetone)$_n$ precipitate was filtered and dried under vacuum to give 5.46 g (10.5 mmol) of pure, white **G$_2$BSPB** (50% yield). ^{1}H NMR (dimethyl sulfoxide-d_6, 400 MHz, *J*/Hz): δ 7.50 (d, 4H, $^2J = 8$, 2-*H*), 6.95 (s, 12H, **G**), 6.86 (d, 4H, $^2J = 8$, 3-*H*), 4.04 (m, 4H, O−CH_2), 1.86 (m, 4H, 1-CH_2).

Crystallography. Experimental parameters pertaining to the single-crystal X-ray analyses are given in Table 2 (see Supporting Information). Data were collected on Bruker SMART APEX II CCD platform diffractometer with graphite monochromated Mo Kα radiation ($\lambda = 0.71073$ Å) at 100(2) K or 200(2) K. The structures were solved by direct methods and refined with full-matrix least-squares/difference Fourier analysis using the APEX2 (fully integrated with SHELX-97) suite of software.[44] All non-hydrogen atoms were refined with anisotropic displacement parameters, and all hydrogen atoms were placed in idealized positions and refined with a riding model. Data were corrected for the effects of absorption using SADABS. The data collection of compound **G$_2$NDS**·$^1/_2$(DTE) was carried out at 15-ID ChemMatCARS beamline, Advanced Photon Source, Argonne National Laboratory, using a Bruker SMART APEXII CCD detector. Data were collected at 100 K with a wavelength of 0.44280 Å with an exposure time of 0.6 s per frame and a crystal-detector distance of 5.5 cm.

Fluorescence. Fluorescence measurements were performed using a Hitachi F-2500 fluorescence spectrophotometer, equipped with a 150 W xenon light source. Liquid samples were placed inside Fisherbrand* disposable polystyrene four-clear-sided cuvettes purchased from Fisher Scientific. In the case of solid samples, several

(41) Clarke, H. T. *J. Org. Chem.* **1971**, *36*, 3816.

(42) (a) Moore, F. J. *J. Am. Chem. Soc.* **1903**, *25*, 622. (b) van Es, T.; Backeberg, O. G.; Morrison, I. *J. South Afr. Chem. Inst.* **1964**, *17*, 95.

(43) Stone, G. C. H. *J. Am. Chem. Soc.* **1936**, *58*, 488.

(44) (a) Sheldrick, G. M. *SHELX-97*; University of Göttingen: Göttingen, Germany, 1997. (b) Sheldrick, G. M. *Acta Crystallogr., Sect. A: Found. Crystallogr.* **2008**, *64*, 112.

single crystals of a given compound were placed at the bottom of a glass NMR tube cut to fit into the cuvette holder of the spectrophotometer. The excitation slit width was set at 2.5 nm. The emission slit widths (2, 5, or 10 nm) were adjusted to enhance intensity values. Data were collected at a scan speed of 300 nm/min and a photomultiplier (PMT) detector voltage of 400 V.

Transmittance and Reflectance Absorption. Both transmittance (for liquid samples placed in quartz cuvette) and reflectance (for solid samples) absorption measurements were performed using a Perkin-Elmer Lambda 950 UV/vis Spectrometer. Reflectance measurements were performed in total reflectance mode by attaching an 8° wedge to the sample port of a 60-mm integrating sphere. All solid crystalline samples were lightly ground into polycrystalline powders, loaded into a 1.25-in. diameter sample cup, mixed with $BaSO_4$ (95% by weight) as a diluent, and pressed firmly to create a smooth sample surface. The sample cup was then attached onto the sample port of the integrating sphere. The UV/vis slit width was fixed at 2 nm. The photomultiplier detector gain was 30, and its integration (response) time was 0.20 s. Absorbance values (A) were converted from % reflectance (%R) according to $A = -\log(\%R)$.

Computational Study. Calculations of the electronic transition energy between the ground and excited (singlet and/or triplet) states were performed with the Gaussian03 program package[45] using time-dependent density functional theory (TDDFT) at the PBE0/6-311G(d,p) level. PBE0 is built on the Perdew−Burke−Ernzerhof pure functional, in which the exchange is weighted (75% DFT/25% Hartree−Fock) accordingly to theoretical considerations. Electronic transition energy calculations for the guests in the inclusion compounds and as isolated molecules were based on molecular geometries extracted from the crystal structures as determined by single crystal X-ray diffraction. In addition, the oscillator strength, *f*, for each electronic transition was calculated. The coefficient *f* is related to the molar extinction coefficient of that transition, and hence the transition with the highest *f* is assigned as the calculated absorption maxima ($\lambda_{max,calc}$) that can be compared with the experimental absorption maxima (λ_{max}). Conformational analysis of the guests was performed using density functional theory (DFT) at the PBE0/6-311G(d,p) level and was based on the geometry-optimized molecular structure of the guests at various predetermined dihedral angles.

Acknowledgment. The authors thank Samuel Hawxwell and Chunhua (Tony) Hu of the New York University Molecular Design Institute, Yu-Sheng Chen of ChemMatCARS, APS, and Charles Campana of Bruker Inc. for their assistance in crystal structure determinations. Bernardo Moltrasio and Maurizio Cossi are acknowledged for helpful suggestions on computational calculations. This work was supported in part by the Fondazione Cariplo and the NSF Division of Materials Research (DMR-0906576). Use of the Advanced Photon Source was supported by the U.S. Department of Energy, Office of Science, Office of Basic Energy Sciences, under Contract No. DE-AC02-06CH11357. ChemMatCARS Sector 15 is principally supported by the National Science Foundation/Department of Energy under grant number CHE-0535644.

Supporting Information Available: Crystal images with face indexing, various schematics of crystal structures and additional structural phase diagrams, ab initio calculation details, individual absorption and emission spectra, structural features of compounds **29**−**32**, crystallographic information files (CIFs), and complete citation for reference 45. This material is available free of charge via the Internet at http://pubs.acs.org.

JA106106D

(45) Frisch, M. J., et al. *Gaussian 03 (Revision C.02)*; Gaussian, Inc.: Wallingford, CT, 2004.